Ocean Dynamics (2012) 62:439–447
DOI 10.1007/s10236-011-0509-1

The use of autonomous underwater vehicles to map the variability of under-ice topography

Peter Wadhams

Received: 20 January 2011 / Accepted: 23 November 2011 / Published online: 8 January 2012

Abstract We review the development of autonomous underwater vehicle (AUV) use under sea ice to map the three-dimensional (3-D) structure of the ice underside. The author, after extensive experience in under-ice profiling from submarines using single-beam sonar, carried out the first under-ice sidescan sonar profiling from an AUV in 2002 in the Greenland Sea. This was followed in August 2004 by the first full multibeam sonar experiment, using Kongsberg EM2000 sonar aboard the Autosub-II vehicle off NE Greenland. Two experiments using a small Gavia vehicle deployed through holes in the ice followed in 2007 and 2008, in the Beaufort Sea and off Ellesmere Island. Examples of the 3-D imagery are shown, and the two approaches of using a large vehicle deployed from a ship and a small through-ice vehicle are compared and found to be complementary. The imagery has shown that although first-year (FY) ridges have the familiar shape of a triangular prism made of small ice blocks, multi-year (MY) ridges are found to be broken up by lead formation into a chain of individual large ice blocks rather than a coherent linear feature. New work and future plans are described.

Keywords Sea ice · Ice thickness · Multibeam sonar · AUV · Pressure ridges · Ice roughness

Responsible Editor: Michel Rixen

This article is part of the Topical Collection on *Maritime Rapid Environmental Assessment*

P. Wadhams (✉)
Department of Applied Mathematics and Theoretical Physics,
University of Cambridge,
Cambridge, UK
e-mail: p.wadhams@damtp.cam.ac.uk

1 Introduction

There are important reasons to know the three-dimensional topography of the under-ice surface. The polar sea ice cover consists of two distinct components: thermodynamic ice, which has reached its current thickness by natural growth; and deformed ice, which can attain a much greater thickness through rafting and ridging. Pressure ridges, formed by the crushing of refrozen leads, can reach a draft of more than 50 m. From the viewpoint of modelling the role of sea ice in climate, this composite nature of the ice cover must be considered in order to deal with dynamics, thermodynamics and mechanics correctly. For the offshore industry, too, ridging is important, as the deepest multi-year (MY) pressure ridge represents the design load on an offshore structure, while the deepest ridges also control ice scouring frequencies in the nearshore zone. The topography of sea ice is important for such diverse applications as calculating its containment potential for oil blowouts, its role as a substrate for a sea ice ecosystem, its impact on icebreaker design, and its scattering potential for under-ice acoustic propagation.

The first measurements of under-ice topography were simple linear profiles generated by narrow-beam upward-looking sonar. These were first obtained from naval submarines, and it was the voyage of USS *Nautilus* in 1958 which first revealed, via an upward sonar profile, the rugged topography of the ice underside with its landscape of steep pressure ridges separated by smoother undeformed floe sections (Lyon 1961). From then on, frequent submarine transects of the Arctic Ocean in different years and seasons have enabled the regional distribution of ice topography to be determined (Bourke and Garrett 1987) and, more recently, the rapid decline in mean ice draft throughout the Arctic to be documented (Rothrock et al. 1999, 2003, 2008; Wadhams 1990; Wadhams and Davis 2000, 2001; Yu et al. 2004).

The present author began conducting ice underside surveys from Royal Naval submarines in 1971, and soon engaged with the problem of the inadequacy of a simple line profile. In 1976 he fitted a sidescan sonar to a submarine and obtained the first sidescan imagery of the under-ice surface (Wadhams 1978a), repeated in 1987 with a better sonar (Wadhams 1988). Sidescan sonar shows the distribution of smooth and ridged ice over the under-ice surface, and by giving the directionality of pressure ridges that cross the submarine track can be used in conjunction with upward sonar to give the true slope angle of a pressure ridge at the point where it crosses the submarine track (Davis and Wadhams 1995). It also enables the two major ice types, first-year (FY) ice and MY ice, to be visually discriminated, in that undeformed FY ice has a very smooth under-ice surface while even undeformed MY ice has a rugged underside caused by uneven melt rates during previous summers due to surface melt pools (Wadhams and Martin 1990; Sear and Wadhams 1992). Sidescan therefore allows a wider analysis to be done of the ice underside than upward sonar alone.

The ultimate solution, however, is a sonar which gives a proper 3-D picture of a swath of ice underside. This was only achieved when multibeam sonar became available. The first use of upward-looking multibeam sonar from a submarine was by the present author in 2007 from HMS *Tireless* (Wadhams 2008) using a Kongsberg EM2000 system. The difference between sidescan and multibeam is that sidescan sonar is simply a fan-shaped beam (sometimes split into separate port and starboard channels) in which the backscattered signal strength from each pulse is plotted against time, being interpreted as slant range. This constructs a map as the vessel proceeds along its track, with strong scatterers showing as bright echoes and shadow zones as dark. Multibeam sonar employs an electronically steered beam which gives individual echoes from 100 to 500 angles of beam emerging from a single ping, building up a quantitative map of the topography of the target surface. In the rest of this paper we review the use of multibeam on autonomous underwater vehicles (AUVs).

2 Mapping the under-ice surface by AUV

Although a naval submarine is in many ways the ideal platform for multibeam sonar because of the large track length that can be obtained from a single voyage, there are reasons for fitting a similar sonar to a smaller vehicle which is completely under the control of the experimenter, i.e., an AUV. These include

1. A submarine must carry out its transect during an operational voyage and therefore the timing and spatial nature of the data gathering are not entirely under the control of the experimenter.
2. In particular, an AUV is capable of carrying out a "lawnmower" pattern of surveys, i.e., a grid with sidelapping, which permits a square area of ice bottom to be mapped rather than a long narrow swath. A submarine can do the same (e.g., HMS *Tireless* in 2007 ran a mosaic of 11 swaths in a region of MY ice N of Greenland), but it is more difficult to achieve both in terms of vessel guidance and in terms of ship-time availability.
3. An AUV can be targeted on a specific ridge, series of ridges, or area of icefield which is being studied from the surface in other ways, e.g., from an ice camp or ice surface survey programme operating in cooperation with the AUV.
4. An AUV can proceed more slowly and at a more shallow depth than a submarine, allowing higher resolution under-ice imagery to be obtained.
5. An AUV can operate in regimes which are dangerous or impossible for a manned submarine, e.g., in shallow water or under ice shelves.

Set against these advantages is the fact that an AUV mission requires the experimenter to provide logistics in harsh conditions (e.g., an ice camp) while a submarine mission can be carried out in apparent comfort and safety (although the 2007 *Tireless* voyage included a fatal explosion).

The earliest AUV experiments under ice were carried in the Beaufort Sea in 1972 using a vehicle called Unmanned Arctic Research Submersible (UARS) equipped with three narrow-beam upward sonars (Francois and Nodland 1972; Francois 1977). This work was far ahead of its time, and the next under-ice use of an AUV was during the winter Lead Experiment (LeadEx) in 1992, in the Beaufort Sea (Morison and McPhee 1998). The 1.6-m-long vehicle carried a CTD but no sonar and was launched and recovered from a lead, homing to an acoustic beacon before recovery in a net. The Canadian Defence Research Establishment (Atlantic) used a large AUV for cable-laying in the Arctic in 1996, but no scientific data were collected (Ferguson et al. 1999). In 2001, single-beam upward sonar data were successfully collected in the Antarctic from the UK Autosub vehicle (Brierley et al. 2002) and in the Arctic from a test cruise of a vehicle developed by Monterey Bay Aquarium Research Institute (Tervalon and Henthorn 2002).

The present author and his team pioneered the collection of 3D data from AUVs under ice, beginning in February 2002 with the use of a Maridan Martin 150 AUV, equipped with a Tritech SeaKing 675-kHz sidescan sonar, a CTD and an ADCP (Wadhams et al. 2004). This vehicle obtained sidescan imagery of the underside of floes in the East Greenland Current, and the upward sonar channel obtained thickness distributions in good agreement with work by submarines.

True quantitative 3-D maps of the ice underside were first obtained in August 2004 using the Autosub II AUV off NE Greenland (Wadhams et al. 2006), where more than 450 track km were imaged using a Kongsberg EM2000 multibeam sonar with 100 m swath width. The same vehicle later collected multibeam sonar data under the Fimbul ice shelf in the Antarctic (Nicholls et al. 2006) before being lost under the same ice shelf.

In addition to these ship-launched AUV missions, we realised that it would be desirable to deploy an AUV through a hole in the ice, enabling the vehicle to target a specific local ice regime or feature. Large AUVs — such as Autosub — are too long and heavy for this application, while mobilisation costs are significant such that extended or repeated deployments become prohibitively expensive. We therefore employed a small, man-handle-able Gavia AUV in April 2007 in the Beaufort Sea and again in April 2008, in the Lincoln Sea, obtaining valuable under-ice sonar images of a specific study area (Wadhams and Doble 2008; Doble et al. 2009), using a GeoSwath sonar system. We summarise results from these large and small AUV operations below.

2.1 Results from Autosub operations

In August 2004, the Autosub-II AUV was taken aboard RRS *James Clark Ross*, and worked on the Greenland continental shelf from 79°N northwards. This shelf contains the shallow Belgica and Ob' Banks. Belgica Bank is very shallow in places and has been found to contain small temporary low-lying islands such as Tobias Island, an ice-push feature resembling Alaskan barrier islands (Mohr and Forsberg 2001). Ridged polar ice from the East Greenland Current grounds on Belgica Bank together with broken-out thin tabular icebergs from nearby Greenland glaciers such as the 79 Glacier and the Zachariae Isstrøm, where a major iceberg breakout was observed in 2003. To the west, the Belgica Bank is separated from the Greenland coast by a system of connected troughs (Belgica, Norske, and Westwind) with outlets to south and north. The shallow bank creates pinning points for a locally grown fast ice sheet that extends across the Norske Trough to the Greenland coast, known as the Norske Øer Ice Barrier (NØIB). Complete breakup of NØIB was once rare, occurring about every 50 years, but since 2002 the NØIB has disintegrated almost every summer (Hughes et al. 2011).

A series of AUV missions was despatched westwards from the Belgica Bank fast ice edge towards the Greenland coast, passing first through the shallow water zone N of the Northwind Shoal, then to the deeper Norske Trough, and close to the Greenland coast. The missions were up to 25 h in duration, i.e., 150 km of track. While Autosub was under the ice the shipboard team ran lines of drilled holes at 5-m intervals along the axis of the vehicle's track near the ice edge and took ice cores. Further work was done from the Westwind Trough, further north.

Some examples of multibeam sonar imagery obtained during the cruise from the Kongsberg EM-2000 multibeam sonar are shown in Fig. 1 (from Wadhams et al. 2006). Each of the displayed images is a perspective view of the underside of ridged ice, obtained at 40 m depth. The scenes are shown illuminated by a sun of elevation 20°. Alongside each image is a probability density function (pdf) of ice draft for the image region compared with a pdf for the entire mission. The ice was a combination of ridges and thick floes frozen into place by ice formed the previous winter. The sonar itself operated at 200 kHz, producing 111 beams with 1.5° beam spacing, over a 120–150° swath. Physically the transducer has dimensions of 18×14×42 cm and a power consumption of 80 W. It is therefore suitable for use only in large AUVs.

Figure 1a shows the deepest ridge encountered, with a maximum depth of 33 m. Since the individual ice blocks which compose ridges are quite small, the ridge itself is a relatively uniform triangle in cross-section, representing the angle of repose of a pile of buoyant ice. Wadhams (1978b) drew attention to this characteristic of ridges deeper than 30 m in an analysis of submarine profiles. A lesser ridge is visible in the foreground. The undeformed ice on the nearside corner of the image is 1.75 m in draft (FY) and between the two ridges is 4 m (MY); it is likely that the giant ridge, the smaller ridge and the intervening ice form part of an embedded floe that has drifted into Belgica Bank from the Arctic Ocean.

Figure 1b is a 100×250 m image also obtained over Belgica Bank. It shows an old MY ridged floe of thickness 3–5 m which is clearly embedded in younger fast ice of draft 1.8 m. The older, thicker floe resembles floes seen in the marginal ice zone (MIZ) of Fram Strait, where large sheets of advecting Arctic sea ice are fractured by wave action and turned into floes of typical diameter 100 m retaining fragments of their original pressure ridges. The edges of the floe are sharp and linear as would occur with a fracture which occurred just before embedding. The ridge which occupies half of the floe has maximum draft 11 m and contains separate ice blocks of typical diameters 5–20 m. Probably before embedding it was in a state of disintegration; observations in the MIZ often show such floes shedding ice blocks from their underside under the impact of waves. The surrounding thinner ice is probably FY ice despite its unusual thickness. The faint pattern of depressions in the underside occurs because of the presence on the upper surface of meltwater pools. These pools preferentially absorb incoming radiation, giving a heat flux which enhances bottom melt and generates a bottom depression which mirrors the pool's position on the top side (Wadhams and Martin 1990; Wadhams 2000). Although the existence of such topographic features has been inferred from topside observations, and their general shape has been revealed by

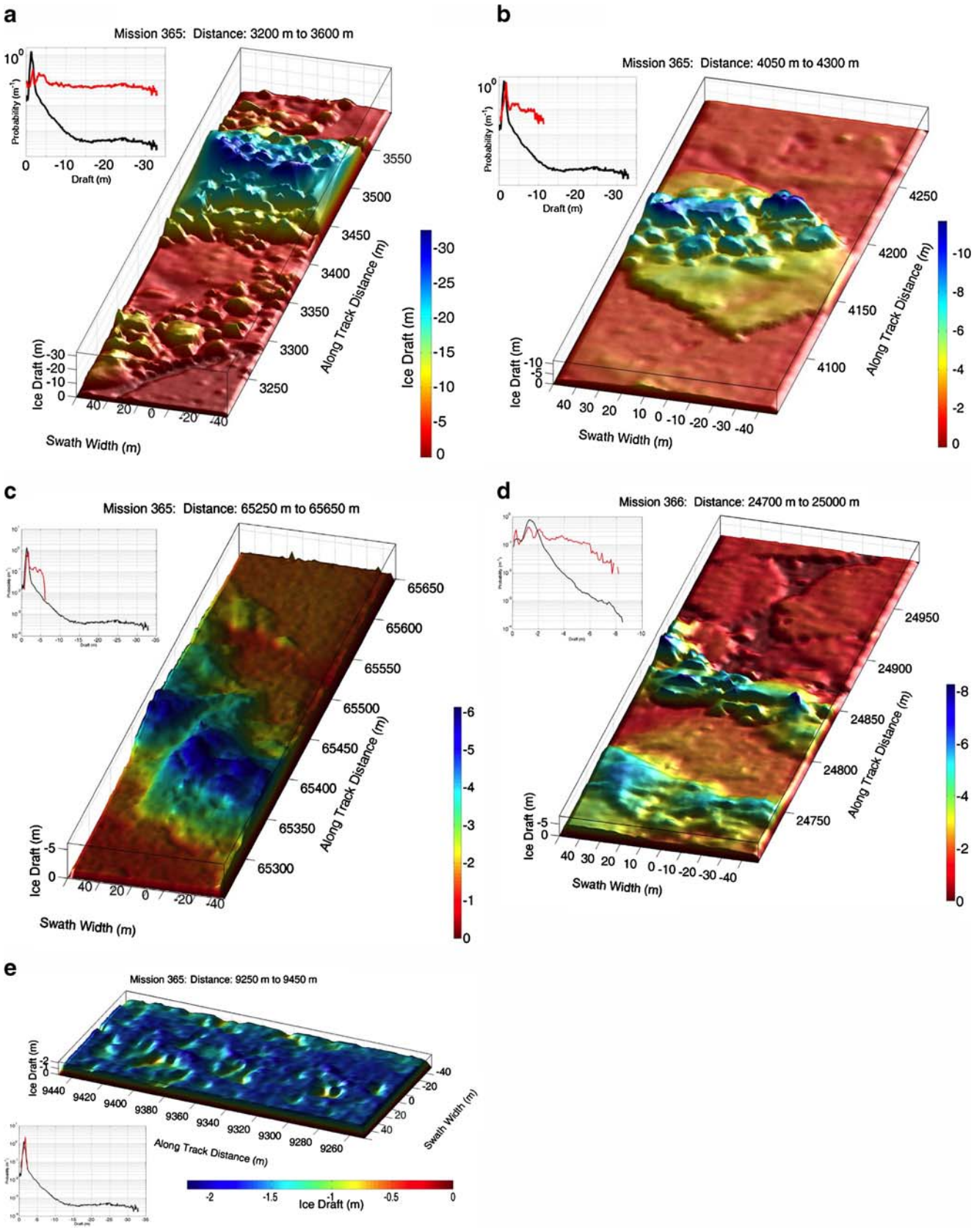
a
Mission 365: Distance: 3200 m to 3600 m
Probability (m⁻¹)
Draft (m)
Ice Draft (m)
Swath Width (m)
Along Track Distance (m)
b
Mission 365: Distance: 4050 m to 4300 m
c
Mission 365: Distance: 65250 m to 65650 m
d
Mission 366: Distance: 24700 m to 25000 m
e
Mission 365: Distance: 9250 m to 9450 m

◀ **Fig. 1** Autosub II cruise to NE Greenland: some examples of EM-2000 multibeam ice draft data in perspective views, as if illuminated by a sun of elevation 20°. Data points fill 2×2 m grid. No vertical exaggeration unless otherwise stated. Each image is accompanied by its probability density function (*pdf*) of ice draft (*red*) compared to the pdf of the mission as a whole (*black*) (lin-log scale, 5-cm bins). **a** Deep 33 m ridge on Belgica Bank, with shallower ridge in foreground, both surrounded by undeformed ice. **b** Thick multi-year ridged floe of draft 3–5 m, with linear edges suggesting production from fracture of larger ice sheet, embedded in undeformed fast ice of draft 1.8 m. Fast ice shows pattern of depressions due to mirroring of surface melt pools. Thicker ice contains pressure ridge of maximum draft 11 m which has partly disintegrated into individual ice blocks of diameter 5–20 m. Evidence is that thicker floe came from MIZ. **c** Pressure ridge from western side of Norske Trough. Maximum draft 6.0 m. Smooth undeformed ice has peaks at 1.7 and 1.3 m. Vertical exaggeration 1.75:1. **d** Image showing in background first-year floes of 1.2 m draft with rounded edges embedded in young ice of 0.25 m draft. In centre is young linear ridge, possibly shear ridge formed between the first-year ice and thicker floe in foreground. Foreground floe is multi-year ice of 1.85–2.25 m draft and in front a worn-down multi-year hummock. Vertical exaggeration 1.25:1. **e** Multi-year undeformed floe which has developed deep craters in underside to match deep surface meltwater pools. Modal draft is 1.7 m, with maximum of 2.2 m and with some craters as thin as 0.5 m. Vertical exaggeration 4:1

sidescan sonar imagery (Wadhams 1988), the quantitative data available here marks a significant advance.

Figure 1c shows an area from an otherwise smooth fast ice regime near the coast of Greenland. It shows a pressure ridge of 6 m draft, the only pressure ridge after more than 30 km of undeformed fast ice. The ridge axis is oriented at 45° to the track of the AUV, and there appears to be a jog in the line of the ridge crest, like a fracture zone in plate tectonics, which is probably due to the opening of a crack accompanied by shear. The fast ice around the ridge has 1.7 m draft, while further to the east, across the trough and bank, it is only 1.0–1.3 m, indicating either that in this western part of Norske Trough, close to the continental influence of Greenland, the ice grows more rapidly, or that unbalanced isostasy in the ridge is affecting the draft of nearby ice.

Figure 1d is an image from Westwind Trough, showing in the background well-rounded FY floes (draft 1.2 m) glued together by very young ice (thickness 0.25 m), with a young (probably FY) ridge in the centre of the image and an old worn-down hummock in the front. Between the two is an MY floe of thickness 1.85–2.25 m containing the hummock. The young ridge is narrower and more clearly linear than that of Fig. 1c and may be a shear ridge rather than a pressure ridge, formed by motion or pressure between the FY ice and the older floe. The contrast between the sharpness of topography in the two ridges is dramatic, showing the effect of a number of years of ageing and partial melt in rounding off the blocky topography of the older ridge.

Figure 1e shows an example of a large undeformed MY floe which has developed a much deeper system of melt pool-associated depressions than the FY ice of Fig. 1b. The contrast between shallow pools (Fig. 1b) and deep craters on the lower surface is because each year the refrozen melt pools from the year before reopen and deepen, causing increased compensating melt on the underside. This image is vertically enhanced to 4:1 to show the crater-like nature of the features. We infer that the floe was multiyear despite a modal draft of only 1.7 m because it lay close to our validation line, where the modal draft was also 1.7 m and where the thickness-averaged salinity of the ice cores was only 0.96 PSU, characteristic of multiyear ice.

The accompanying pdfs are of particular interest. The advantage of the multiple beam system (the electronic equivalent of 111 parallel beams) is that good quality pdfs can be obtained over shorter distances than the 50 km commonly employed for single-beam upward sonar. The improvement is not as great as is suggested by the number of beams, of course. The multibeam image is equivalent to 111 parallel profiles of the ice underside, and if these were independent a given quality of pdf could be obtained in $1/\sqrt{111}$ (less than 10%) of the track length needed for a single-beam pdf. However, since the correlation length of ice roughness is about 100 m (Wadhams 2000) a use of strictly independent beams might only involve the centre beam and two outer beams being used to generate the pdf, which only gives an improvement of $\sqrt{3}$ over single beam data.

The pdfs do yield new information about ice draft distribution. Hitherto it was known from long upward sonar profiles that the pdf has a tail with a negative exponential form (Wadhams 2000) but now we see that this is created by the superposition of a series of top hat functions (e.g., Fig. 1a, b, c), each due to a single ridge, which are flat as far as an ultimate drop-off depth, as would be expected from a basically triangular geometry. The overall pdf approaches a negative exponential from 3- to 10-m draft but then flattens out as the only contribution to deeper ice comes from the single ridge.

The westward missions towards the coast of Greenland also achieved some significant oceanographic discoveries. Firstly (Fig. 2), we found that the bathymetry available from International Bathymetric Chart of the Arctic Ocean (IBCAO), itself updated in 2001, was deficient, showing deeper water over Belgica Bank and shallower water over Norske Trough than found by Autosub, and also much less detailed topography. Autosub showed the Norske Trough to be at least 460 m deep near its western end, while the IBCAO bathymetry shows 200 m. The ADCP data across the Norske Trough showed that at the centre of the trough, at water depths from the surface to 100 m, there is a strong northward current component of 0.2–0.25 ms^{-1}, while near Belgica Bank, at water depths of 100–120 m, there is a strong southward component of 0.15–0.25 ms^{-1}. The shelf circulation in this area was first described by Bourke et al. (1987) and refined by the International Arctic Polynya Programme (Hirche and Deming 1997; Schneider and Budéus 1997). They defined a

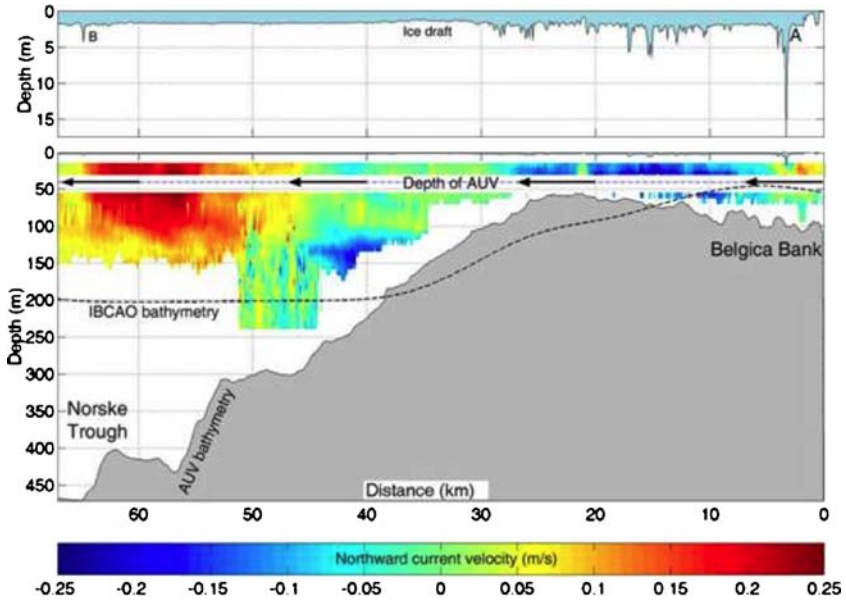

Fig. 2 The outward track of mission 365, 21–22 August 2004, run at 40 m depth. The top profile is ice draft measured at crude resolution by upward-looking ADCP. **a**, **b** Ridges shown in Fig. 3 whose depths are underestimated by the ADCP. Note smooth undeformed ice over Norske Trough. The bottom profile is the seabed topography measured by Autosub compared with the IBCAO bathymetry (*dashed line*). The *coloured masses* are N–S velocity components measured by the downward looking ADCP aboard Autosub. The *red* area is a strong northward current in the Trough, the Northeast Greenland Coastal Current (*NGCC*); the blue area is a hitherto unrecognised southward current on the western flank of Belgica Bank

northward-flowing Northeast Greenland Coastal Current (NGCC) within the trough system. We can identify the northward current seen by Autosub with the NGCC but the southward current is a hitherto unrecognized counter-current.

2.2 Results from through-ice AUV operations

The Gavia vehicle used for the first operation at the APLIS-2007 camp (Applied Physics Laboratory Ice Station) was 3.1 m long, weighed only 80 kg in air, and was chosen as being capable of being launched by hand. It was fitted with a GeoSwath 500 kHz interferometric sonar system built by GeoAcoustics Ltd. of Great Yarmouth, UK. The sonar is normally used to look downwards at the seafloor, but for under-ice operations the vehicle was ballasted to run inverted so that all instruments looked upwards at the ice underside. For navigation, the vehicle was equipped with a Kearfott IN-24 inertial navigation system (INS), coupled to a doppler velocity log (DVL) which tracked its progress across the ice underside.

The experiments formed part of the SEDNA project led by University of Alaska, Fairbanks (UAF), a multi-sensor survey of the region around a camp which was originally established near 73°N, 145°W by the Arctic Submarine Laboratory, San Diego, as a base for acoustic experiments with US and British submarines. The AUV measurements benefited from multiple validation studies by other sensors including a submarine survey of the site carried out by *Tireless* in March 2007 during her first multibeam survey operation. AUV surveys were done coincidently with laser profilometer (freeboard) and electromagnetic induction (thickness) overflights.

Two sites were used for the AUV experiments. The first, for calibration, was a region of mainly undeformed FY ice which did not contain well-defined ridges. The second site was close to an FY ridge which was observed to have formed on April 2, 8 days before our work began. This was a much more complex topography, and the subject of intense surface studies by the UAF group. In each case, a 3×1 m hole was melted by a hot water drill, which allowed the AUV to be floated horizontally and made ballasting and mission preparation easier. A heated canvas hut mounted on a sled was placed over the hole. This was also much safer than trying to operate from some natural stretch of open water, e.g., a lead or floe edge, which might close up. The Gavia's acoustic homing system did not function, so at all times the vehicle was attached to a tether line, which restricted its range.

The imagery shown here (Fig. 3) was obtained at the second site, beside a recently formed pressure ridge in FY ice. MY ice lay within range of the AUV to the west (top of image) and a thin (48 cm draft) refrozen lead lay to the right of the ridge. Several cross-sections of the ridge near the AUV hole were surveyed by drilling by the UAF team. The experimental strategy was to send out the AUV along a track to a distance of 100–300 m from the hole, make a wide turn and return to the hole. The return run was usually deeper than the outward leg, to ensure that the tether line was pulled down, away from any obstructions (the line was also slightly negatively buoyant).

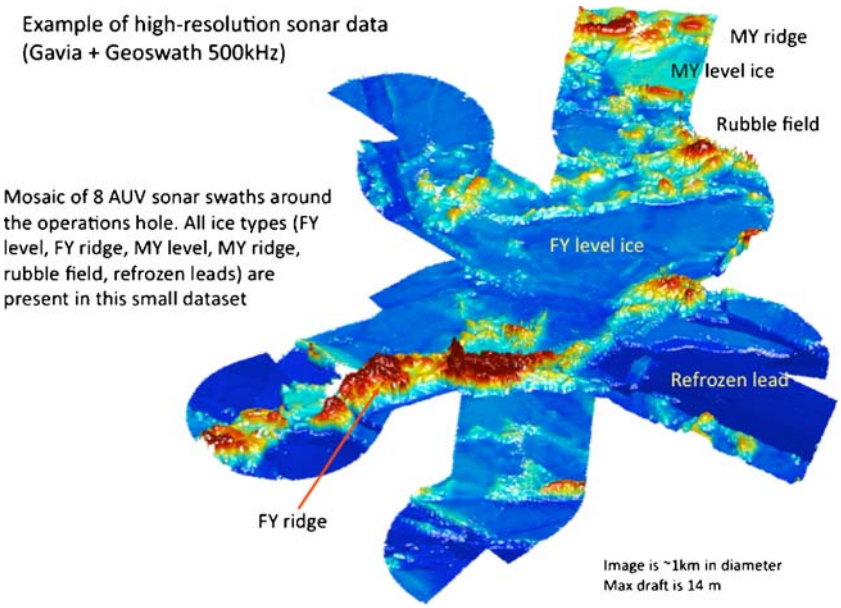

Fig. 3 Gavia AUV study 2007: sonar data gathered around the deployment hole, showing a refrozen lead, a young pressure ridge, FY level ice, a rubble field, and an MY pressure ridge. The contrasting roughness and shapes of FY and MY ridging is clearly shown. Running depth of the vehicle was 20 m

The data shown in Fig. 3 were obtained by synthesizing several runs, and two distinct types of ridge are shown in some detail. The main study ridge, next to the ice hole, was up to 14 m deep and runs from left to right across the lower centre of the image. It is a very young ridge which had been observed to form only about 8 days before the measurements were done. We see the classic shape of an FY ridge, with a continuous crest and a triangular cross-section, composed of small ice blocks piled randomly and loosely. FY ice forms most of the level area (modal draft 1.6 m), then an associated rubble field (modal draft 2.4 m) towards the top right of the plot and a refrozen lead to the lower right (modal draft 0.85 m). Most extraordinary, however, is the region just within range of the vehicle, at the extreme top of the image. Out of an area of MY level ice (modal draft 2.9 m) emerges an 8.8 m draft MY ridge. The contrast between the old, rounded, solid ice blocks of the MY ridge and the small piled-up blocks of the FY ridge is particularly striking, and can be compared with a FY/MY ridge juxtaposition in Fig. 1d. It can be seen that the ageing process, rather than simply solidifying the ridge structure and smoothing its outer shape, has inserted a succession of cracks (opening into refrozen leads) across the crest line of the ridge, breaking it up into a chain of individuals large blocks. The ridge is clearly more formidable than the FY ridge, but is also more discontinuous.

The final experiment reported here was done on fast ice north of the Canadian Forces base at Alert, Ellesmere Island (82°33′N, 62°34′W) in early May 2008, again using a Gavia vehicle and GeoSwath sonar (Doble et al. 2009). A camp was established in a region of heavily deformed MY ice on the edge of an FY ice zone, and a tent set up over an ice hole as in 2007. Figure 4 shows the composite ice draft map produced by the AUV sonar system, from several passes. It

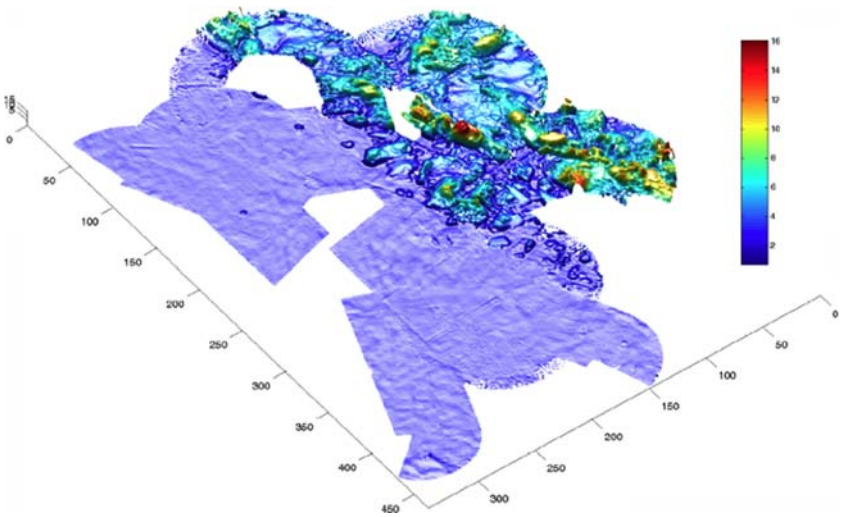

Fig. 4 Ice draft in ridged MY ice zone beside FY ice north of Ellesmere Island, May 2008. Note very large isolated block in centre and some evidence of lineation on right. Scales: all marked scales, vertical and horizontal, are in metres

can be seen that there is some evidence of linearity, but that basically the deformed MY ice is broken up into a number of large blocks which have become displaced to such an extent that one can no longer think in terms of a linear pressure ridge. We believe that a mechanism for this is that an initially linear ridge suffers periodic modification as long-distance cracks (opening into leads) propagate across the ridge. As each crack opens into a lead and refreezes, it breaks the continuity of the ridge crest. If the lead formation is accompanied by shear, it also breaks the linearity. Over a period of many years, so many such events occur that there no longer remains any long undisturbed stretch of ridge crest. The individual blocks have become solid because through melt and refreeze the original small ice blocks have evolved into a single massif; the typical form of an MY ridge is thus a string of solid blocks rather than a single linear structure. The suggestion is that such a ridge would have less strength in interacting with structures than a complete linear ridge.

2.3 Recent developments and future plans

During November–December 2010, new work was carried out in the Antarctic, with results not yet reported. A Gavia system was used by A. Forrest and M. Doble to study the under-ice and under-shelf surface near the Erebus Glacier Tongue, while H. Singh (Woods Hole Oceanographic Institution [WHOI]) used a double-hulled WHOI AUV with multibeam to study sea ice in the Bellingshausen Sea from RRS *James Clark Ross*. First results indicate that observed pressure ridges were formed by buckling of existing ice floes rather than by crushing and the creation of small ice blocks, in agreement with other observations of a differing behaviour in Antarctic sea ice ridging (Wadhams 2000).

The present author and his team plan new work using both large and small AUVs. In terms of climate change studies, data gathering is intended to do the following:

- Study how the *complete thickness distribution responds to melt*. We will examine both spatial and temporal variations in the thickness distribution.
- *Validate and calibrate large-scale thickness measuring techniques* which have the potential for routinely monitoring ice thickness on regional and global scales in the future, by performing co-incident measurements with airborne electromagnetic and scanning laser profilometer instruments.

The deployment programme is designed to target critical areas:

- *Beaufort Sea*, where the major loss of ice extent (seen in 2007, 2008 and 2009) occurred. A suitable platform is the APLIS series of ice camps.
- *Lincoln Sea*, north of Greenland and Ellesmere Island, which (a) contains the thickest ice in the Arctic, including most of the surviving MY ice; (b) is the "switchyard" for ice and water, which can variously exit the Arctic through Fram Strait or Nares Strait, or be re-circulated back into the Arctic via the Beaufort Sea. An operation here would be run from Alert and involve collaboration with the ESA CryoSat cal-val programme.
- *Fram Strait/East Greenland Current*: the major export pathway of Arctic sea ice.
- *Antarctic*, where baseline data are scarce.

Other equipment besides multibeam, ADCP and video can be fitted to an AUV. The WHOI vehicle, for instance, has been tested with a mass spectrometer for detecting chemical species under ice (e.g., oil slicks), and we aim to develop such applications further.

3 Conclusions

The programmable nature of an AUV renders it ideal for targeted studies in concert with other measurements, whether by alternative platforms or in situ techniques. Additionally, the AUV can perform measurements in areas where a manned submarine cannot venture, either because of safety concerns (shallow water, ice shelves) or exclusion by Treaty (the Antarctic).

A large AUV like Autosub can operate very successfully over relatively long distances. It can undertake necessary avoidance manoeuvres for obstacles, and the acoustic homing system ensures that the vehicle returns with confidence to an area where it can surface. The combination of a large unmanned under-ice vehicle and a multibeam sonar gives, literally, a new dimension to under-ice studies and is extremely valuable for large-scale surveys.

By contrast, the use of an AUV that is small enough to be manhandled enables its deployment in almost any field context — from ice camps, offshore structures, ships or aircraft touchdowns. All that is needed is the ability to make a suitable hole, a source of power for recharging batteries (e.g., a petrol generator), and, desirable but not essential, a tent or hut to cover the hole. One can then deploy the vehicle near a feature of special interest and survey its three-dimensional underside topography with great accuracy and high resolution. Improvements in acoustic homing for small vehicles returning to small holes will be necessary for safe operation without tethers.

We wish to emphasise this contrast between two types of mission — large-scale and local — and between two accompanying types of deployment — from a ship, and through an ice hole. It is not absolutely the case that only small vehicles can be launched from ice holes, e.g., a large

Explorer-class AUV was launched from an ice hole for an UNCLOS seabed mapping mission in 2010 (Crees et al. 2010), but economics and practical considerations are strongly supportive of using a hole for a local mission but, where possible, a ship for a long-range mission.

Results of high-definition multibeam profiling so far point to a fundamental difference in shape between FY and MY ridges. This is not so much a difference in average ridge slope as a difference in crest continuity, with FY ridges approximating to linear triangular prisms while MY ridges are broken up by the intervention of leads into a sequence of individual ice blocks, sometimes losing all evidence of ridge linearity. This has implications for the forces which an MY ridge can exert on an offshore structure.

It is important to continue to develop optimum AUV–sonar combinations for the serious task of mapping the changing ice cover, in particular to follow the changes in topography and under-ice structure which accompany the thinning currently being experienced by Arctic sea ice. Deployment of this sensor combination to study the very different under-ice topography of the Antarctic is also bound to be most fruitful.

References

Bourke RH, Garrett RP (1987) Sea ice thickness distribution in the Arctic Ocean. Cold Regions Sci Technol 13:259–280

Bourke RH, Newton JL, Paquette RG, Tunnicliffe MD (1987) Circulation and water masses of the East Greenland Shelf. J Geophys Res 92:6729–6740

Brierley AS, Millard NW, McPhail SD, Stevenson P, Pebody M, Perrett J, Squires M, Griffiths G (2002) Antarctic krill under sea ice: elevated abundance in a narrow band just south of ice edge. Science 295:1890–1892

Crees T, Kaminski C, Ferguson J, Laframboise JM, Forrest A, Williams J, MacNeil E, Hopkin D, Pederson R (2010) UNCLOS under ice survey – an historic AUV deployment in the Canadian high arctic. *OCEANS* 1–8

Davis NR, Wadhams P (1995) A statistical analysis of Arctic pressure ridge morphology. J Geophys Res 100(C6):10915–10925

Doble MJ, Forrest AL, Wadhams P, Laval BE (2009) Through-ice AUV deployment: operational and technical experience from two seasons of Arctic fieldwork. Cold Regions Sci Technol 56:90–97

Ferguson J, Pope A, Butler B, Verrall R (1999) Theseus AUV: two record-breaking missions. Sea Technol, 65–70, February

Francois RE (1977) High resolution observations of under-ice morphology. Univ. Washington, Applied Physics Lab., Tech. Rept. APL-UW 7712, p. 30.

Francois, R.E. and W.K. Nodland (1972). Unmanned Arctic Research Submersible (UARS) system development and test report. Univ. Washington, Applied Physics Lab., Tech. Rept., APL-UW 7219, p. 88

Hirche H-J, Deming JW (eds) (1997) Northeast Water Polynya symposium. J Mar Syst 10(1–4)

Hughes NE, Wilkinson JP, Wadhams P (2011) Multi-satellite sensor analysis of fast-ice development in the Norske Øer Ice Barrier, northeast Greenland. Ann Glaciol 52(57), in press.

Lyon WK (1961) Ocean and sea-ice research in the Arctic Ocean via submarine. Trans N Y Acad Sci 2(23):662–674

Mohr JJ, Forsberg R (2001) Searching for new islands in sea ice. Nature 416:351

Morison JH, McPhee MG (1998) Lead convection measured with an autonomous underwater vehicle. J Geophys Res 103(C2):3257–3281

Nicholls KW, Abrahamsen EP, Buck JJH, Dodd PA, Goldblatt C, Griffiths G, Heywood KJ, Hughes NE, Kaletzky A, Lane-Serff GF, McPhail SD, Millard NW, Oliver KIC, Perrett J, Price MR, Pudsey CJ, Saw K, Stansfield K, Stott MJ, Wadhams P, Webb AT, Wilkinson JP (2006) Measurements beneath an Antarctic ice shelf using an autonomous underwater vehicle. Geophys Res Lett 33: L08612. doi:10.1029/2006GL025998

Rothrock DA, Yu Y, Maykut GA (1999) Thinning of the Arctic sea-ice cover. Geophys Res Lett 26(23):3469–3472

Rothrock DA, Zhang J, Yu Y (2003) The arctic ice thickness anomaly of the 1990s: A consistent view from observations and models. J Geophys Res 108(C3):3083. doi:10.1029/2001JC001208

Rothrock DA, Percival DB, Wensnahan M (2008) The decline in arctic sea-ice thickness: Separating the spatial, annual, and interannual variability in a quarter century of submarine data. J Geophys Res 113:C05003. doi:10.1029/2007JC004252

Schneider W, Budéus G (1997) Summary of the Northeast Water Polynya formation and development (Greenland Sea). J Mar Syst 10:107–122

Sear CB, Wadhams P (1992) Statistical properties of Arctic sea ice morphology derived from sidescan sonar images. Prog Oceanogr 29:133–160

Tervalon NS, Henthorn R (2002) Ice profiling sonar for an AUV: experience in the Arctic. OCEANS'02, MTS/IEEE, 1:305–310

Wadhams P (1978a) Sidescan sonar imagery of sea ice in the Arctic Ocean. Can J Remote Sens 4:161–173

Wadhams P (1978b) Characteristics of deep pressure ridges in the Arctic Ocean. POAC 77. Proc. 4th Intl. Conf. on Port & Ocean Engineering under Arctic Conditions, St. John's, I, 544–555, Memorial Univ. Newfoundland

Wadhams P (1988) The underside of Arctic sea ice imaged by sidescan sonar. Nature 333:161–164

Wadhams P (1990) Evidence for thinning of the Arctic ice cover north of Greenland. Nature (Lond) 345:795–797

Wadhams P (2000) Ice in the ocean. Taylor and Francis, London, p 368

Wadhams P (2008) Arctic sea ice changes under global warming. Proc. ICETECH 2008, Intl.Conf. on Performance of Ships and Structures in Ice, Banff, July 20–23 2008. Soc. Naval Archit. Marine Engineers, ISBN 978-0-9780896-1

Wadhams P, Davis NR (2000) Further evidence of ice thinning in the Arctic Ocean. Geophys Res Lett 27:3973–3975

Wadhams P, Davis NR (2001) Arctic sea-ice morphological characteristics in summer 1996. Ann Glaciol 33:165–170

Wadhams P, Doble MJ (2008) Digital terrain mapping of the underside of sea ice from a small AUV. Geophys Res Lett 35(L01501), doi:10.1029/2007GL031921

Wadhams P, Martin S (1990) Processes determining the bottom topography of multiyear Arctic sea ice. In Ackley SF, Weeks WF (eds) Sea ice properties and processes. US Army Cold Regions Res Eng Lab, Hanover NH, Monograph 90–1, 136–141

Wadhams P, Wilkinson JP, Kaletzky A (2004) Sidescan sonar imagery of the winter marginal ice zone obtained from an AUV. J Amos Oceanic Technol 21(9):1462–1470

Wadhams P, Wilkinson JP, McPhail SD (2006) A new view of the underside of Arctic sea ice. Geophys Res Lett 33:L04501. doi:10.1029/2005GL025131

Yu Y, Maykut GA, Rothrock DA (2004) Changes in the thickness distribution of Arctic sea ice between 1958–1970 and 1993–1997. J Geophys Res 109:C08004. doi:10.1029/2003JC001982